Design and Evaluation of a New General-Purpose Device for Calibrating Instrumented Spatial Linkages

Joshua A. Nordquist
Department of Mechanical Engineering,
University of California,
One Shields Avenue,
Davis, CA 95616

M. L. Hull[1]
Department of Mechanical Engineering,
and Biomedical Engineering Program,
University of California,
One Shields Avenue,
Davis, CA 95616
e-mail: mlhull@ucdavis.edu

Because instrumented spatial linkages (ISLs) have been commonly used in measuring joint rotations and must be calibrated before using the device in confidence, a calibration device design and associated method for quantifying calibration device error would be useful. The objectives of the work reported by this paper were to (1) design an ISL calibration device and demonstrate the design for a specific application, (2) describe a new method for calibrating the device that minimizes measurement error, and (3) quantify measurement error of the device using the new method. Relative translations and orientations of the device were calculated via a series of transformation matrices containing inherent fixed and variable parameters. These translations and orientations were verified with a coordinate measurement machine, which served as a gold standard. Inherent fixed parameters of the device were optimized to minimize measurement error. After parameter optimization, accuracy was determined. The root mean squared error (RMSE) was 0.175 deg for orientation and 0.587 mm for position. All RMSE values were less than 0.8% of their respective full-scale ranges. These errors are comparable to published measurement errors of ISLs for positions and lower by at least a factor of 2 for orientations. These errors are in spite of the many steps taken in design and manufacturing to achieve high accuracy. Because it is challenging to achieve the accuracy required for a custom calibration device to serve as a viable gold standard, it is important to verify that a calibration device provides sufficient precision to calibrate an ISL.
[DOI: 10.1115/1.2965375]

1 Introduction

Instrumented spatial linkages (ISLs) have been used widely for measuring the total (i.e., six degrees of freedom) relative motion between body segments [1–14]. These relative motions represent those of joints, which have included the knee, ankle, and wrist, all of which are primarily rotational joints (Table 1). Relative motions with an ISL are calculated through matrix multiplication of a series of transformation matrices. These transformation matrices are derived from mechanical and electrical parameters of an ISL.

To use an ISL in confidence, the device must be calibrated and the measurement error quantified. Calibrating an ISL involves measuring the relative position and orientation of known calibration points and optimizing the mechanical and electrical parameter values to minimize measurement error [12,14–17]. Calibration points are created with a calibration device, which mechanically joins with an ISL. Measurement error can then be quantified by comparing ISL position and orientation results with known calibration point position and orientation quantities.

Calibration devices have been developed in the past for each particular ISL design. Suntay et al. [14] developed a single degree-of-freedom calibration device, which simulated the ISL's measurement application (knee joint flexion). Kirstukas et al. [15] developed a four degree-of-freedom calibration device, which also simulated the expected measurement application (motion of the knee). Because most human joints allow primarily rotations [18] a general-purpose calibration device, which is designed specifically for the application of joint rotations and is adaptable for ISLs of varying size, shape, and workspaces, would be beneficial to improving the accuracy of measuring anatomical joint rotations with an ISL. Thus the first objective of this study was to design a calibration device, which meets these criteria, and demonstrate an example device for a specific application.

Any calibration device must also be calibrated and the error quantified to serve as a viable standard for calibration of an ISL. Similar to calibrating an ISL, calibrating a calibration device involves measuring the relative position and orientation of its calibration points and optimizing any necessary parameter values to minimize error. The calibration device must be calibrated with a "gold standard," which is another device that has inherent position and orientation errors substantially lower than that of the calibration device. Although previous studies have documented the accuracy of ISLs [1,11,14–16,19], none have documented the accuracy of their calibration device. The second objective was to describe a new method for calibrating our general-purpose calibration device that minimizes error of the device. The related final objective was to determine the error of the calibration device using this new method. Because an ISL and attendant calibration device are application specific and because ankle joint motion is of interest, the above objectives were accomplished using an example calibration device suitable for an ISL to measure ankle joint motion [20].

2 Materials and Methods

2.1 Design Description. The design of our ISL calibration device, which meets the necessary criteria, is a kinematic chain of three revolute joints whose axes are mutually perpendicular (Fig. 1). All three axes intersect at a point, the center of rotation (COR), allowing simulation of an approximate three degree-of-freedom spherical joint. Fixation points for an ISL were offset from the center of rotation to appropriate locations to allow the center of rotation to be located at the approximate anatomical center of the ankle joint complex (AJC).

The calibration device was designed and manufactured with the goal of offering sufficient precision in both position and orientation for calibrating an ISL. Components were manufactured from 6065 series aluminum utilizing a numerically controlled (NC) milling machine with a resolution in digital readout of 0.0025 mm (Model CV500, Mori Seiki, Japan) and a manual lathe with a resolution in digital readout of 0.025 mm (Model Colchester 13 in., Clausing, Kalamazoo, MI). NC milling machine programs were created via computer-aided manufacturing (CAM) software, FEATURECAM 9 (EGS, Salt Lake City, UT). Revolute joints were constructed using a double-bearing compression design, minimizing play from bearings and machining tolerances (Fig. 2). Stainless steel, flanged, sealed, and raised inner race bearings were chosen to allow side loading of the bearing without hindering rotational motion. Fixation for the ISL onto the calibration device was achieved using a cylindrical *C*-clamp design, maximizing

[1]Corresponding author.

Contributed by the Bioengineering Division of ASME for publication in the JOURNAL OF BIOMECHANICAL ENGINEERING. Manuscript received October 16, 2006; final manuscript received June 25, 2008; published online January 7, 2009. Review conducted by Phillip V. Bayly.

Table 1 A summary of ISLs used in previous research (NA indicates that the information was not documented in the respective publication)

Author(s)	Year	Joint of interest	Calibration device used	Calibration device error (only if calibrated)		ISL error	
				Position (mm)	Orientation (deg)	Position (mm)	Orientation (deg)
Townsend	1977	Knee	No	NA	NA	NA	NA
Chao	1980	Hip, knee, ankle	Yes	NA	NA	NA	1.6
Suntay et al.	1983	Knee	Yes	NA	NA	0.5	0.5
Kirstukas et al.	1992	Knee	Yes	NA	NA	0.7	0.4
Siegler et al.	1996	Ankle	Yes	NA	NA	0.5	1.2
Sholukha et al.	2004	NA	Yes	NA	NA	0.8	0.7

contact area to eliminate play from machining tolerances between two mating components.

The ISL measurement application dictated the range of motion of the example calibration [20]. The example device allows for ± 30 deg of flexion/extension, ± 15 deg of internal/external rotation, and ± 15 deg of inversion/eversion. These ranges cover those previously measured for the ankle joint [10,21].

Revolute joint rotations were controlled via highly accurate linear micrometers (Model V63MRL, 0–50 mm, 0.002 mm resolution, Starrett, Athol, MA). The micrometers were offset from the revolute joint center, forming a three-bar linkage (a triangle) (Fig. 3). Rotation values β_i were calculated via the law of cosines:

$$\beta_i = \cos^{-1}\left(\frac{\text{bar1}_i^2 + \text{bar2}_i^2 - (\text{micro}_i + \text{madj}_i)^2}{2 \cdot \text{bar1}_i \cdot \text{bar2}_i}\right) + \text{offset}_i \quad (1)$$

where bar1_i and bar2_i are fixed-length sides of a triangle, micro_i is the readout of the micrometer head (the third side of the triangle), offset_i resets the rotation values to zero at the neutral position, madj_i is the micrometer installation tolerance, and i is an index representing a revolute joint of the calibration device. All fixed-value design parameters (bar1_i, bar2_i, offset_i, madj_i) were optimization parameters whose values were adjusted during optimization to minimize measurement error (Table 2).

Calibration device fixed and moving coordinate systems were then established with the origins at each ISL fixation point. Relative position and orientation between the fixed and moving coordinate systems were calculated via transformation matrices. Transformation matrices were created via the Denavit–Hartenberg system of parameters [22] and a systematic approach for developing transformation matrices of linkages [6,23]. The four Denavit–Hartenberg parameters are joint offset a_i, twist angle α_i, link length s_i, and revolute angle θ_i. The transformation matrix was calculated with these four parameters, allowing transformation to the i frame from the $i-1$ frame, where i denotes a link of the calibration device as follows:

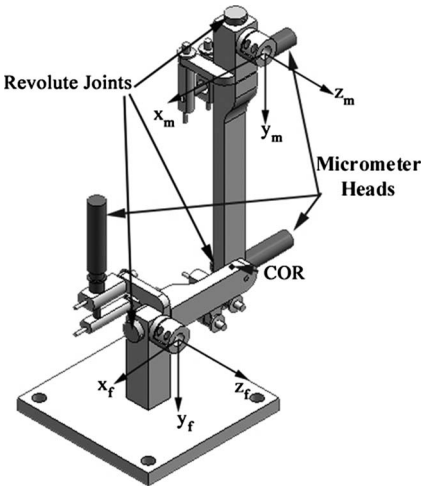

Fig. 1 Illustration of the calibration device. The device has three degrees of freedom with three revolute axes that intersect at the center of rotation (COR). Also illustrated are the fixed (*f*) and moving (*m*) coordinate systems. In the illustration the calibration device is in the defined neutral position.

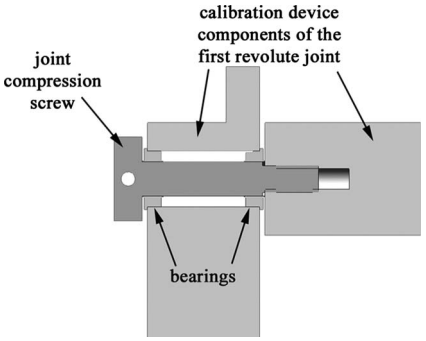

Fig. 2 Illustration of the revolute joint design. Revolute joints in the calibration device were constructed with a double-bearing compression design. The joint compression screw, when tightened, minimized any play in the joint due to machining and assembly tolerances.

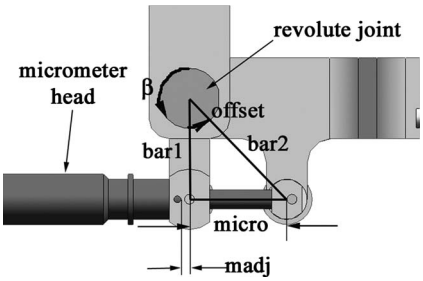

Fig. 3 Illustration of the three-bar linkage and necessary parameters for controlling the rotation about the revolute joint. The micrometer varied the distance "micro" to control rotation. Additional revolute joints, which connected the micrometer to bar1 and bar2, utilized brass bushings and a lock nut compression design to minimize play from machining tolerances. The micrometer was installed using set screws and created the third link with a line contact (i.e., end of micrometer contacted cylindrical surface) to ensure proper micrometer measurement. Lastly, the three-bar linkage was energized with a spring (not shown for clarity) across the micrometer to eliminate play.

$$[T^{i/i-1}] = \begin{bmatrix} 1 & 0 & 0 & 0 \\ -a_i \cos\theta_i & \cos\theta_i & \cos a_i \sin\theta_i & \sin a_i \sin\theta_i \\ a_i \sin\theta_i & -\sin\theta_i & \cos a_i \cos\theta_i & \sin a_i \cos\theta_i \\ -s_i & 0 & \sin a_i & \cos a_i \end{bmatrix} \quad (2)$$

Four additional coordinate systems were necessary to establish a chain of transformation matrices calculating the relative position and orientation between the fixed and moving coordinate systems according to

$$[T^{f/m}]_{CS} = [T^{f/4}]_{CS} \cdot [T^{4/3}]_{CS} \cdot [T^{3/2}]_{CS} \cdot [T^{2/1}]_{CS} \cdot [T^{1/m}]_{CS} \quad (3)$$

where f and m denote the fixed and moving coordinate systems, respectively. The three position and three orientation components of relative motion were determined by equating the resulting transformation matrix to that of a general six-parameter (three orthogonal positions and three ordered orthogonal orientations) transformation matrix given by

$$[T^{f/m}]_{CS} = \begin{bmatrix} 1 & 0 & 0 & 0 \\ r_1 & \cos\phi_1 \cos\phi_2 - \sin\phi_1 \sin\phi_2 \sin\phi_3 & -\sin\phi_1 \cos\phi_3 & \cos\phi_1 \sin\phi_2 + \sin\phi_1 \cos\phi_2 \sin\phi_3 \\ r_2 & \sin\phi_1 \cos\phi_2 + \cos\phi_1 \sin\phi_2 \sin\phi_3 & \cos\phi_1 \cos\phi_3 & \sin\phi_1 \sin\phi_2 - \cos\phi_1 \cos\phi_2 \sin\phi_3 \\ r_3 & -\sin\phi_2 \cos\phi_3 & \sin\phi_3 & \cos\phi_2 \cos\phi_3 \end{bmatrix} \quad (4)$$

where r_1, r_2, and r_3 are the three relative position components (i.e., coordinates of the origin of the moving coordinate system in the fixed coordinate system) and ϕ_1, ϕ_2, and ϕ_3 are the three relative orientation components (i.e., ordered sequence of angles to orient the moving coordinate system coincident with the fixed coordinate system) between the fixed and moving coordinate systems. The sequence order followed the subscripts of the angles.

The orientation components corresponded to anatomical rotations of the ankle joint complex. For the right leg, ankle flexion was given by angle ϕ_1 and was a rotation about the positive z_m axis, internal rotation was given by angle ϕ_3 and was a rotation about the positive y_f axis, and inversion was given by angle ϕ_2 and was a rotation about an axis, which was mutually perpendicular to the z_m and y_f axes [3]. Relative orientations between fixed and moving coordinate systems were zero at the neutral position. The neutral position was defined as 0 deg flexion/extension, 0 deg inversion/eversion, and 0 deg internal/external rotation, as it applies to the anatomical ankle joint complex (Fig. 1).

Twenty-nine optimization parameters were necessary to completely describe the relative position and orientation between the established fixed and moving coordinate systems (Table 2, Figs. 3 and 4). Of the five necessary transformations between the six coordinate systems, three included the revolute joint rotation β_i as the Denavit–Hartenberg paremeter θ_i. Revolute joint rotation, β_i, depended on four optimization parameters (Eq. (1)), increasing the number of optimization parameters for transformations including revolute joint rotation from 4 to 7. There were three revolute joint rotations (21 optimization parameters) and the remaining transformations (2) had 4 optimization parameters each ($21 + 4 \cdot 2 = 29$).

Table 2 List of the 29 linkage parameters and their values before and after optimization

Parameters	Initial guess	Optimized	Difference	Unit
p10	0.0000	0.8331	0.8331	mm
r10	0.0000	−0.0431	−0.0431	rad
p20	−35.5600	−32.5167	3.0433	mm
r20	0.0000	0.0036	0.0036	rad
p11	0.0000	0.8169	0.8169	mm
r11	1.5708	1.5490	−0.0218	rad
p21	−238.7346	−236.7196	2.0150	mm
bar11	42.5970	42.5541	−0.0429	mm
bar21	38.6255	39.1717	0.5462	mm
madj1	7.8000	7.7962	−0.0038	mm
offset1	0.6288	0.6314	0.0026	rad
pl2	0.0000	1.2521	1.2521	mm
r12	1.5708	1.6466	0.0758	rad
p22	0.0000	−0.0844	−0.0844	mm
bar12	44.0120	45.2126	1.2006	mm
bar22	31.7500	31.7889	0.0389	mm
madj2	9.7300	8.9669	−0.7631	mm
offset2	0.8058	0.8632	0.0574	rad
p13	0.0000	−0.7924	−0.7924	mm
r13	1.5708	1.5311	−0.0397	rad
p23	101.6000	102.1555	0.5555	mm
bar13	42.5970	41.9676	−0.6294	mm
bar23	38.6255	37.8316	−0.7939	mm
madj3	7.8000	7.8588	0.0588	mm
offset3	0.6288	0.6615	0.0327	rad
p1f	0.0000	−0.9310	−0.9310	mm
r1f	1.5708	1.6130	0.0422	rad
p2f	35.5600	34.1097	−1.4503	mm
r2f	1.5708	1.5629	−0.0079	rad

2.2 Calibration and Error Analysis. The calibration device was statically calibrated with a coordinate measuring machine (CMM) (Model BRT504, Mitutoyo, Auroro, IL). The CMM is a three linear-axis device with a documented precision of 0.0005 mm, which was more than sufficient to serve as a viable gold standard. Four calibration quantities described below were measured for each of 125 randomly selected calibration points. A calibration point was defined as a unique combination of the three positions and three orientations describing the relative position and orientation between the moving and fixed coordinate systems. Calibration points were produced with unique combinations of micrometer adjustments. Five values were chosen for each micrometer, which included the minimum, maximum, and neutral values for each revolute joint (± 30 deg, 0 deg flexion/extension, ± 15 deg, 0 deg abduction/adduction, and ± 15 deg, 0 deg internal/external rotation). Five revolute joint angle values for each of the three revolute joints provided a total of 125 calibration points. One hundred of the measured calibration points were used for a least-squares parameter optimization. Including a large number of points in the calibration resulted in a larger reduction in error [15]. The remaining 25 points were used to compute statistics (i.e., average error or bias and standard deviation of error or random error) to quantify the measurement error of the calibration device.

The four calibration quantities were chosen so that measurement error would be minimized. These calibration quantities consisted of three orientation measurements and one position measurement. The three orientation measurements were inverse

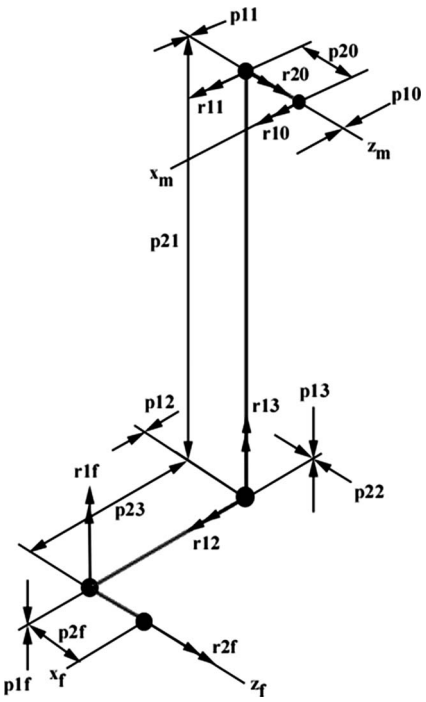

Fig. 4 Diagram illustrating 17 of the 29 optimization parameters for the calibration device. Figure 3 illustrates the remaining 12. Double arrows pointing in the same direction represent rotations while arrows pointing in opposite directions at a line indicate parameters (e.g., p1f) with an initial value of 0.

direction cosines between a unit vector representing the z axis of the moving coordinate system and the three axes of the fixed coordinate system (Fig. 1). z axes for both the moving and fixed coordinate systems were measured with the CMM as the central axis of a cylinder installed onto the calibration device in the same manner as the ISL. Calculation of the central axis unit vector was via an algorithm provided within CMM software (GEOPAK, Mitutoyo, Aurora, IL). The remaining two fixed coordinate axes were measured with the CMM as vectors normal to existing planes of the calibration device, which are parallel to the x and y fixed coordinate axes (Fig. 5). The three coordinate system unit vectors were checked to be orthogonal and were within 0.2 deg. The position measurement was the magnitude of a vector from the origin of the fixed coordinate system to the origin of the moving coordinate system. Origins of the fixed and moving coordinate systems were measured with the CMM as the intersection of each respective z axis and the respective perpendicular ISL installment planes (Fig. 5).

Differences between the calibration quantities measured with the CMM and calibration quantities calculated via the 29 optimization parameters (termed calibration residuals) were included in the cost function for optimization. Calculated calibration quantities were found by partitioning the transformation matrix (Eq. (4)) for the calibration device into two partitions, a position partition and an orientation partition as follows:

$$[T^{f/m}]_{\mathrm{CS}} = \begin{bmatrix} I & 0 \\ [P^{f/m}]_{\mathrm{CS}} & [R^{f/m}]_{\mathrm{CS}} \end{bmatrix} \tag{5}$$

where $P^{f/m}$ represents the position partition and $R^{f/m}$ represents the orientation partition. A unit vector representing the moving coordinate system z axis was calculated as the product of the fixed coordinate system z axis unit vector ($\mathbf{u}_{zf}$) and the orientation partition. Inverse direction cosines were calculated by taking the dot product of respective fixed coordinate system axis unit vectors

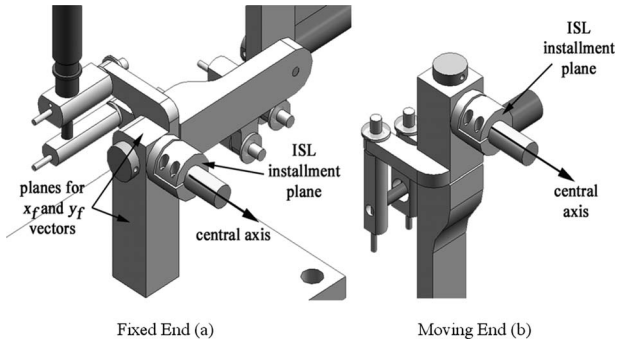

Fig. 5 Illustrated are the features of the calibration device measured with the CMM for the purpose of identifying calibration points. (*a*) is the fixed end of the device and (*b*) is the moving end of the device.

($\mathbf{u}_{xf}$, $\mathbf{u}_{yf}$, $\mathbf{u}_{zf}$) with the moving coordinate system z axis vector (Eqs. (6)–(8)).

$$\mathrm{IDC}_x = \cos^{-1}(([R^{f/m}]_{\mathrm{CS}} \cdot \mathbf{u}_{zf}) \cdot \mathbf{u}_{xf}) \tag{6}$$

$$\mathrm{IDC}_y = \cos^{-1}(([R^{f/m}]_{\mathrm{CS}} \cdot \mathbf{u}_{zf}) \cdot \mathbf{u}_{yf}) \tag{7}$$

$$\mathrm{IDC}_z = \cos^{-1}(([R^{f/m}]_{\mathrm{CS}} \cdot \mathbf{u}_{zf}) \cdot \mathbf{u}_{zf}) \tag{8}$$

where IDC denotes inverse direction cosine and the subscript f denotes fixed coordinate system axes. The calculated position measurement P was determined as the magnitude of the subposition matrix.

$$P = \sqrt{r1^2 + r2^2 + r3^2} \tag{9}$$

The differences between these calculated quantities and those measured with the CMM (i.e., calibration residuals) are denoted as RS. In the cost function J calibration residuals were normalized to full-scale range (FSR), squared, weighted (wt_P as a position weighting and wt_O as an orientation weighting), and then combined as follows:

$$J_{\mathrm{CS}} = \sum_{j=1}^{n} \left(\mathrm{wt}_o \left(\left(\frac{\mathrm{RS}_{\mathrm{IDC}x}}{\mathrm{FSR}_{\mathrm{IDC}x}} \right)^2 + \left(\frac{\mathrm{RS}_{\mathrm{IDC}y}}{\mathrm{FSR}_{\mathrm{IDC}y}} \right)^2 + \left(\frac{\mathrm{RS}_{\mathrm{IDC}z}}{\mathrm{FSR}_{\mathrm{IDC}z}} \right)^2 \right) + \mathrm{wt}_p \left(\frac{\mathrm{RS}_p}{\mathrm{FSR}_p} \right)^2 \right)_j^2 \tag{10}$$

where n denotes the total number of calibration points and j denotes an individual calibration point. Values for weighting were chosen to be between 0 and 1 at 0.1 intervals, and both wt_O and wt_P were related according to

$$\mathrm{wt}_O + \mathrm{wt}_P = 1 \tag{11}$$

Optimization of the 29 parameters was performed using a nonlinear least-squares algorithm. The algorithm is a subspace trust region method and is based on the interior-reflective Newton method [24,25]. Iterations of the algorithm involve the approximate solution of a large nonlinear system (the transformation matrix calculation involving the 29 optimization parameters) using the method of preconditioned conjugate gradients. Calculations were performed with computational software (MATLAB 6, The Mathworks, Natik, MA) and custom-designed programs for calculations unique to the calibration device. Convergence criteria of the optimization routine were the maximum number of iterations (1,000,000), minimum change in the cost function ($1e^{-12}$), or minimum value of the cost function ($1e^{-12}$). These values were recorded and evaluated after each iteration of the optimization.

Using optimized parameter values, error analysis residuals were calculated in the same manner as the calibration residuals, differing only in that the remaining calibration points (not used for

Table 3 Measures of calibration device accuracy computed from the calibration and accuracy check (All percent are relative to the scale range of the respective performance measure)

Performance measure	P (mm)	RS_{IDCx}(deg)	RS_{IDCy}(deg)	RS_{IDCz}(deg)
RMSE	0.5874	0.1145	0.2269	0.1639
FSR	88.98	24.5210	35.9920	20.1700
%FSR	0.660%	0.467%	0.630%	0.813%

parameter optimization) were utilized. Root mean squared errors (RMSEs) were calculated for each of the four calibration quantities. The RMSEs were compared for values of wt_O between 0 and 1 at 0.1 intervals. The value of wt_O that yielded the lowest RMSE values yielded the optimized parameter set for the calibration device.

3 Results

Parameter optimization converged, according to the convergence criteria, in 33,333 iterations (Table 2). Results of the optimization were reported via the MATLAB software, concluding that the minimum change in the cost function was reached.

Using optimized parameters, the RMSE in vector length P was 0.5874 mm (Table 3), which is 0.660% of FSR. Inverse direction cosine RMSEs were 0.1145 deg, 0.2269 deg, and 0.1639 deg (Table 3) for RS_{IDCx}, RS_{IDCy}, and RS_{IDCz}, respectively. Inverse direction cosine errors are 0.423%, 0.630%, and 0.813% of FSR, respectively. These results were found using a wt_O of 0.5, which yielded the best RMSE results.

4 Discussion

Although numerous calibration devices for ISLs have been constructed and used to minimize and quantify ISL measurement error, no previous study known to the authors has quantified and/or minimized the measurement error of a calibration device independent of an ISL. Therefore the objectives of this study were to (1) design a general-purpose calibration device and demonstrate such a device for a specific application, (2) describe a new method for minimizing and quantifying the measurement error, and (3) minimize and quantify measurement error using this method. The key findings were (1) a three degree-of-freedom calibration device was designed and manufactured using methods to ensure high precision, (2) a method using a CMM was created to minimize and quantify the measurement error, and (3) the RSME was less than 0.8% FSR for both translations and orientations. Because the precision of the calibration device is tied directly to the steps taken in design, manufacturing, and calibration to reduce measurement error, the design, manufacturing, and calibration methods will be critically evaluated followed by a discussion of the results.

To fully quantify the measurement error of an ISL, the inherent measurement error of a calibration device must be known. Calibration devices typically incorporate commercially available components as controls (e.g., linear micrometers, rotational variable differential transformers (RVDTs), etc.) and manufactured components [15,19]. Controls have a documented error (i.e., measurement resolution) while manufactured components have an error that depends on the design tolerances and the ability of the manufacturing method to achieve those tolerances. Accordingly, measurement error of a calibration device is a combination of control error (which is documented) and manufacturing error (which is unknown). Therefore, the measurement error of any calibration device should be quantified to use the device to calibrate an ISL in confidence. Additionally, the calibration device must be considered a gold standard, which offers accuracy preferably an order of magnitude better than that of the ISL. This is to ensure that error of the calibration device does not contribute measurably to the error of the ISL.

Numerous efforts were taken in the design, manufacturing, and calibration of this calibration device so that it would serve as a gold standard to calibrate an ISL. A minimal number of components were utilized in the design while still offering calibration over six degrees of freedom. This was accomplished by using three offset revolute axes to vary all six relative measurement components (three translations and three orientations) for each calibration point. The design was further simplified by restricting the size of an ISL that can be accommodated. For the device to accept ISLs of varying sizes, links of the device must be manufactured to custom lengths. Lastly, the design incorporated methods such as joint compression in the assembly to minimize any play due to assembly of components.

Each component of the device was manufactured using high-precision tools. Most components were machined from solid aluminum with a NC-controlled milling machine with a resolution in digital readout of 0.0025 mm. Remaining components were manufactured with a manual lathe with a resolution in digital readout of 0.025 mm.

A CMM was chosen as the gold standard for calibrating the calibration stand. The CMM is a three linear-axis machine, which translates a stylus tip above the object to measure (varying CMM x and y axes) and then lowers to impact the object (varying CMM z axis). Location of a stylus tip within the CMM's coordinate space is recorded when it impacts with a solid object (i.e., the measured part). With a documented precision of 0.0005 mm, the CMM offered more than sufficient accuracy to serve as a viable gold standard to determine the measurement error of the calibration device.

Calibration measurements were chosen that could be measured with the CMM for every calibration point and uniquely described each calibration point. Because the three relative positions between the fixed and moving ends of the calibration device could not be measured separately, the vector length, P, was chosen (Eq. (9)). Although not unique mathematically, the vector length, P, was unique for each end point of our calibration device. Therefore this length was included along with three inverse direction cosines of the moving end to reflect error in position as well as orientation.

Measurement errors for other ISL calibration devices have not been documented, and therefore cannot be used to compare with error results of our calibration device. However, the accuracy of our device can be compared with previously published accuracy results for ISLs. The measurement error of our calibration device is better by about a factor of 2 in rotations and comparable in translations to measurement errors published for previous ISLs (compare Tables 1 and 3). Despite our efforts taken in the design, manufacturing, and calibration to minimize measurement error of the device, the measurement error precludes using our device to serve as a gold standard for calibrating an ISL particularly in position. Consequently a custom ISL calibration device that offers sufficient accuracy to serve as a gold standard is challenging to produce.

Similar multidegree-of-freedom ISL calibration devices will be subject to comparable measurement errors. The implication is that past ISLs calibrated with a multidegree-of-freedom device could be more accurate than documented. The documented levels of measurement errors for these past ISLs may be due in part to the errors inherent in the calibration device, particularly for ISLs calibrated independently from the calibration device.

Because our calibration device does not offer the accuracy necessary to serve as a gold standard for calibrating an ISL, it is useful to suggest an alternative method that will. Although many alternatives are possible, one is to capitalize on the accuracy of the CMM. The CMM has a documented accuracy that suggests that it can be used as a calibration device for an ISL although it is still

necessary to have a device to interact with both the ISL and the CMM that orients the ISL in all the necessary calibration points. While the calibration device described herein is useful for this purpose, modifications of our calibration device are necessary to create physically measurable coordinate systems at the fixed and moving ends. For example, six spheres of precisely known diameter can be mounted to each coordinate axis. Sphere centers can be measured with the CMM and coordinate systems for both the fixed and moving ends can be created knowing the location of these centers. These coordinate systems will allow all six relative measurements (three positions and three orientations) to be determined directly via the CMM. Additionally, it is necessary to ensure that all six spheres are measurable with the CMM for all calibration points because the CMM stylus tip orientation with respect to the CMM machine cannot be varied without recalibrating the machine. Therefore, all points measured with the CMM (i.e., any area where the stylus tip will impact) must be visible in the CMM *x*-*y* plane (i.e., the calibration stand *x*-*z* plane).

5 Conclusions

In summary, the contributions of this work are several. Two are that a new general-purpose calibration device for manipulating ISL end points has been presented and a new method for minimizing and quantifying the measurement error inherent to this device has been described. Although the RSME of the calibration device was less than 0.8% full-scale range for both positions and orientations, this calibration device provided errors comparable to those of previously published ISLs for positions and lower by at least a factor of 2 for orientations. Thus a third contribution of our work demonstrates that it is challenging to produce a custom calibration device, which offers sufficient accuracy to serve as a gold standard. Accordingly a fourth contribution demonstrates the need to determine the accuracy of any custom calibration device. Because the ISL is the most commonly used goniometer for measuring multidegree-of-freedom motion in joints, these contributions are all important in advancing the usefulness of this goniometer in a broad spectrum of applications.

Acknowledgment

Special thanks are owed to Leo Palaima and Mike Akahori of the UC Davis Student/Faculty Machine Shop for their assistance and support in manufacturing. Also, we acknowledge Mori Seiki Corporation of Japan for providing the CNC milling machine utilized in this project.

References

[1] Chao, E., 1980, "Justification of Triaxial Goniometer for the Measurement of Joint Rotation," J. Biomech., **13**, pp. 989–1006.
[2] Engebretsen, L., Lew, W. D., Lewis, J. L., and Hunter, R. E., 1989, "Knee Mechanics After Repair of the Anterior Cruciate Ligament. A Cadaver Study of Ligament Augmentation," Acta Orthop. Scand., **60**, pp. 703–709.
[3] Grood, E. S., and Suntay, W. J., 1983, "A Joint Coordinate System for the Clinical Description of Three-Dimensional Motions: Application to the Knee," ASME J. Biomech. Eng., **105**, pp. 136–144.
[4] Ishii, Y., Terajima, K., Koga, Y., Takahashi, H. E., Bechtold, J. E., and Gustilo, R. B., 1998, "Gait Analysis After Total Knee Arthroplasty: Comparison of Posterior Cruciate Retention and Substitution," J. Orthop. Sci., **3**, pp. 310–317.
[5] Ishii, Y., Terajima, K., Terashima, S., and Matsueda, M., 2000, "Joint Proprioception in the Elderly With and Without Hip Fracture," J. Orthop. Trauma, **14**, pp. 542–545.
[6] Kinzel, G. L., Hillberry, B. M., Hall, A. S. J., Van Sickle, D. C., and Harvey, W. M., 1972, "Measurement of the Total Motion Between Two Body Segments. II. Description of Application," J. Biomech., **5**, pp. 283–293.
[7] Kirstukas, S. J., Lewis, J. L., and Erdman, A. G., 1992, "6R Instrumental Spatial Linkages for Anatomical Joint Motion Measurement. I. Design," ASME J. Biomech. Eng., **114**, pp. 92–100.
[8] Kovaleski, J. E., Gurchiek, L. R., Heitman, R. J., Hollis, J. M., and Pearsall, A. W. T., 1999, "Instrumented Measurement of Anteroposterior and Inversion-Eversion Laxity of the Normal Ankle Joint Complex," Foot Ankle Int., **20**, pp. 808–814.
[9] Lewis, J. L., Lew, W. D., and Schmidt, J., 1988, "Description and Error Evaluation of an In Vitro Knee Joint Testing System," ASME J. Biomech. Eng., **110**, pp. 238–248.
[10] Siegler, S., Chen, J., and Schneck, C. D., 1988, "The Three-Dimensional Kinematics and Flexibility Characteristics of the Human Ankle and Subtalar Joints--Part I: Kinematics," ASME J. Biomech. Eng., **110**, pp. 364–373.
[11] Siegler, S., Lapointe, S., Nobilini, R., and Berman, A. T., 1996, "A Six-Degrees-of-Freedom Instrumented Linkage for Measuring the Flexibility Characteristics of the Ankle Joint Complex," J. Biomech., **29**, pp. 943–947.
[12] Sommer, H. J. I., and Miller, N. R., 1980, "A Technique for Kinematic Modeling of Anatomical Joints," ASME J. Biomech. Eng., **102**, pp. 311–317.
[13] Townsend, M. A., Izak, M., and Jackson, R. W., 1977, "Total Motion Knee Goniometry," J. Biomech., **10**, pp. 183–193.
[14] Suntay, W. J., Grood, E. S., Hefzy, M. S., Butler, D. L., and Noyes, F. R., 1983, "Error Analysis of a System for Measuring Three-Dimensional Joint Motion," ASME J. Biomech. Eng., **105**, pp. 127–135.
[15] Kirstukas, S. J., Lewis, J. L., and Erdman, A. G., 1992, "6R Instrumental Spatial Linkages for Anatomical Joint Motion Measurement. II. Calibration," ASME J. Biomech. Eng., **114**, pp. 101–110.
[16] Sholukha, V., Salvia, P., Hilal, I., Feipel, V., Rooze, M., and Jan, S. V., 2004, "Calibration and Validation of 6 DOFs Instrumented Spatial Linkage for Biomechanical Applications: A Practical Approach," Med. Eng. Phys., **26**, pp. 251–260.
[17] Sommer, H. J. I., and Miller, N. R., 1981, "A Technique for the Calibration of Instrumented Spatial Linkages Used for Biomechanical Kinematic Measurements," J. Biomech., **14**, pp. 91–98.
[18] Kinzel, G. L., and Gutkowski, L. J., 1983, "Joint Models, Degrees of Freedom, and Anatomical Motion Measurement," ASME J. Biomech. Eng., **105**, pp. 55–62.
[19] Liu, W., and Panjabi, M. M., 1996, "On Improving the Accuracy of Instrumented Spatial Linkage System," J. Biomech., **29**, pp. 1383–1385.
[20] Nordquist, J., and Hull, M. L., 2007, "Design and Demonstration of a New Instrumented Spatial Linkage for Use in a Dynamic Environment: Application to Measurement of Ankle Rotations During Snowboarding," ASME J. Biomech. Eng., **129**, pp. 231–239.
[21] Chen, J., Siegler, S., and Schneck, C. D., 1988, "The Three-Dimensional Kinematics and Flexibility Characteristics of the Human Ankle and Subtalar Joint—Part II: Flexibility Characteristics," ASME J. Biomech. Eng., **110**, pp. 374–385.
[22] Uicker, J. J., Denavit, J., and Hartenberg, R. S., 1964, "An Iterative Method for the Displacement Analysis of Spatial Mechanisms," ASME J. Appl. Mech., **31**, pp. 309–314.
[23] Kinzel, G. L., Hall, A. S. J., and Hillberry, B. M., 1972, "Measurement of the Total Motion Between Two Body Segments. I. Analytical Development," J. Biomech., **5**, pp. 93–105.
[24] Coleman, T. F., and Li, Y., 1994, "On the Convergence of Reflective Newton Methods for Large-Scale Nonlinear Minimization Subject to Bounds," Math. Program., **67**, pp. 189–224.
[25] Coleman, T. F., and Li, Y., 1996, "An Interior, Trust Region Approach for Nonlinear Minimization Subject to Bounds," SIAM J. Optim., **6**, pp. 418–445.